Coordination Chemistry Reviews 255 (2011) 938–948

Contents lists available at ScienceDirect

Coordination Chemistry Reviews

journal homepage: www.elsevier.com/locate/ccr

Review

Theory and spectroscopy of an incarcerated quantum rotor: The infrared spectroscopy, inelastic neutron scattering and nuclear magnetic resonance of $H_2@C_{60}$ at cryogenic temperature

Salvatore Mamone[a], Judy Y.-C. Chen[b], Rangeet Bhattacharyya[a], Malcolm H. Levitt[a], Ronald G. Lawler[c], Anthony J. Horsewill[d], Toomas Rõõm[e], Zlatko Bačić[f], Nicholas J. Turro[b,*]

[a] School of Chemistry, University of Southampton, University Road, Southampton SO17 1BJ, UK
[b] Department of Chemistry, Columbia University, New York, NY 10027, USA
[c] Department of Chemistry, Brown University, Providence, RI 02912, USA
[d] School of Physics and Astronomy, University of Nottingham, Nottingham NG7 2RD, UK
[e] National Institute of Chemical Physics and Biophysics, Akadeemia tee 23, Tallinn 12618, Estonia
[f] Department of Chemistry, New York University, New York, NY 10003, USA

Contents

1. Introduction 938
2. Quantum dynamics of $H_2@C_{60}$ 940
3. Populations of the energy levels of ortho-H_2 and para-H_2 at thermal equilibrium 942
4. IR spectroscopy of $H_2@C_{60}$ at low temperatures 942
5. Inelastic neutron scattering of $H_2@C_{60}$ at low temperatures 944
6. Nuclear magnetic resonance of $H_2@C_{60}$ at low temperatures 945
7. Conclusions 947
8. A coda 947
Acknowledgements 948
References 948

ARTICLE INFO

Article history:
Received 17 August 2010
Accepted 20 December 2010
Available online 11 January 2011

Keywords:
Hydrogen
Fullerene
C_{60}
$H_2@C_{60}$
Confined rotor
Quantum dynamics

ABSTRACT

The supramolecular complex, $H_2@C_{60}$, represents a model of a quantum rotor in a nearly spherical box. In providing a real example of a quantum particle entrapped in a small space, the system cuts to the heart of many important and fundamental quantum mechanical issues. This review compares the predictions of theory of the quantum behaviour of H_2 incarcerated in C_{60} with the results of infrared spectroscopy, inelastic neutron scattering and nuclear magnetic resonance. For $H_2@C_{60}$, each of these methods supports the quantization of translational motion of H_2 and the coupling of the translational motion with rotational motion and provides insights to the factors leading to breaking of the degeneracies of states expected for a purely spherical potential. Infrared spectroscopy and inelastic neutron scattering experiments at cryogenic temperatures provide direct evidence of a profound quantum mechanical feature of H_2 predicted by Heisenberg based on the Pauli principle: the existence of two nuclear spin isomers, a nuclear spin singlet (para-H_2) and a nuclear triplet (ortho-H_2). Nuclear magnetic resonance is capable of probing the local lattice environment of $H_2@C_{60}$ through analysis of the H_2 motional effects on the ortho-H_2 spin dynamics (para-H_2, the nuclear singlet state, is NMR silent). In this review we will show how the information obtained by three different forms of spectroscopy join together with quantum theory to create a complementary and consistent picture which strikingly shows the intrinsically quantum nature of $H_2@C_{60}$.

Published by Elsevier B.V.

1. Introduction

The supramolecular complex $H_2@C_{60}$ (Fig. 1), represents a felicitous marriage of the simplest molecule of all, H_2, with one of the most symmetric and intellectually charming molecules, the fullerene C_{60}. The profound quantum properties and nature of H_2

Abbreviations: IR, infrared; INS, inelastic neutron scattering; NMR, nuclear magnetic resonance; ssNMR, solid state nuclear magnetic resonance; PES, potential energy surface; CSA, chemical shift anisotropy.

* Corresponding author. Tel.: +1 212 567 0189; fax: +1 212 932 1289.
E-mail address: njt3@columbia.edu (N.J. Turro).

0010-8545/$ – see front matter. Published by Elsevier B.V.
doi:10.1016/j.ccr.2010.12.029

Fig. 1. Structure of the $H_2@C_{60}$ supramolecular complex.

are concealed by its apparent simplicity. For example, the prediction of the existence of two distinct allotropes (isomeric forms of a single element) of molecular hydrogen was an early triumph of quantum mechanics [1]. The quantum basis for the two forms is as follows: H_2 is composed of two sets of identical spin 1/2 particles, two protons and two electrons. Both electrons and protons are therefore fermions. The Pauli principle requires the total molecular wave-function of H_2 to be antisymmetric for exchange of the space and spin coordinates of the two indistinguishable protons. The proton spins can combine in a symmetric way to give a total nuclear spin of 1 or in an antisymmetric way to give a total nuclear spin of 0. In a diatomic molecule, with no net electronic angular momentum and spin, the spatial symmetry for exchange of the nuclei is dictated by the integer quantum number $j = 0, 1, \ldots$ which describes its rotational state, according to the parity $(-1)^j$. As a result, in the electronic ground state, para-H_2 (antisymmetric singlet spin function) is required to be associated with rotational functions that are symmetric ($j = 0$, even), and ortho-H_2 (symmetric triplet spin function) is required to be associated with rotational wavefunctions that are antisymmetric (j = odd). The two hydrogen allotropes have distinct physical and chemical properties. At ordinary temperatures hydrogen at equilibrium is a statistical mixture of triplet ortho-H_2 and singlet para-H_2. In general the measurable quantities of H_2 are determined by the relative abundance of the ortho and para species which, in case of slow interconversion, depends on the history of the sample. Farkas' book [2] is an excellent introduction to the basic theoretical aspects and early experimental observations of spin isomerism and spin interconversion in molecular hydrogen isotopomers (including the ortho and para forms of D_2).

The entrapment of H_2 in the confining potential of C_{60} is determined by the supramolecular non-covalent interactions between the H_2 molecule and the carbon atoms of the wall of C_{60}. The confinement of H_2 inside C_{60} leads to quantization of the three translational degrees of freedom associated with the centre of mass motion of H_2. The two lowest rotational levels of free H_2 are separated by $\sim$120 cm^{-1}. These features lead to the expectation that the motional dynamics of H_2 inside C_{60} will be characterized by highly quantum mechanical behaviour. As a result, important issues for theory and experiment are: (1) What is the quantitative extent of quantization of the translational degrees of freedom of $H_2@C_{60}$? (2) What is the magnitude of the coupling of the rotational and translational degrees of freedom of H_2 in C_{60}? (3) How good is the agreement of theory and experiment? (4) How can spectroscopic measurements provide direct or indirect information on issues 1–3?

In this review we address the above issues by describing the current state of theory of the potential energy surface of $H_2@C_{60}$ and the predictions from theory on the quantization of translational degrees of freedom, the coupling of translational and rotational degrees of freedom and the removal of degeneracies of levels that are expected for a perfect spherical potential. We then describe how infrared spectroscopy, inelastic neutron scattering and nuclear magnetic resonance spectroscopy, all at temperatures near 4 K, provide a means of examining the validity of the theory through measurement of energy shifts and energy splittings. In addition, we show how these methods provide a splendid direct means of validating the existence of the ortho-H_2 and para-H_2 and the slowness of interconversion of these two Pauli spin isomers.

The soccer ball shaped C_{60} is the prototype of carbon fullerene molecules forming stable closed structures with nanometer sizes. More precisely C_{60} has the form of a truncated icosahedron and belongs to the highest molecular symmetry point group I_h, thereby realizing the closest approximation to a spherical molecule. An important question that will be discussed in this review is how does the small deviation from perfect spherical symmetry modify the quantum nature of H_2 inside the closed structure, i.e., does the small reduction in symmetry cause measurable breaking of degeneracies that are predicted in the perfect spherical model?

With its diameter of approximately 7 Å, it is natural to consider the possibility of inserting atoms and small diatomic molecules inside the C_{60} cavity. The first endohedral compounds were obtained by inserting noble gas atoms in C_{60} under extreme temperature and pressure conditions [3–7]. However, only a small fraction of the fullerenes, in the order of 10^{-3}, is occupied through this method. Komatsu and co-workers paved the way to the production of $H_2@C_{60}$ in macroscopic quantities through a completely synthetic organic approach [8–10]. In a series of controlled reaction steps they first produced through organic synthesis a large orifice in C_{60}, then inserted H_2 through the orifice at high temperature and pressure and finally "sewed" the hole up back to C_{60} while retaining the hydrogen molecule inside. Almost 100% of the fullerenes were filled with H_2 at the end of this organic synthetic manipulation, now known as *molecular surgery*. In addition to H_2, mixtures of endohedral fullerenes with a predetermined ratio of H_2, HD and D_2 can be prepared. Another interesting class to be mentioned here is constituted by endohedral metallofullerenes, in which a fullerene cage encapsulates clusters that would not be stable otherwise, in particular trimetallnitride complexes inside C_{80} [11–13] and $C_2Sc_2@C_{84}$ [14,15] which is a remarkable example of planar quantum rotor.

The availability of high purity $H_2@C_{60}$ in relatively large amounts (milligrams to grams) greatly expanded the possible applications and fundamental research related to the quantum behaviour of endohedral fullerene complexes. The quantum dynamics of the trapped H_2 is expected to be affected by the confinement in at least two important ways. First, the translational motion associated with the molecular centre of mass becomes unambiguously quantized because of the confinement in the nanoscopic host C_{60}. Thus, the continuum of translational states imposed on the purely rotational states characterized by the energy levels of "free" H_2 split into sets of translational sublevels, all but the first of which, possess various degrees of degeneracies. The small mass of hydrogen combined with the small size of the internal void space of C_{60} and the weak non-covalent bonding between the guest and host, implies large energy spacings and sparseness of the quantized translational and rotational levels. Second, confinement induced couplings between the translational and the rotational motion complicate further the structure of the energy levels: the rotational–translational sublevels split and shift with patterns that reflect the symmetry and the energy related to the size of the confinement.

The high, nearly spherical symmetry of C_{60} is helpful, but not essential, in reducing the mathematical complexity of the computational problem. Thus, the theoretical analysis is simplified and the interpretation of spectroscopic data in terms of the energy of the transitions between the quantized modes of the confined hydrogen becomes apparent. On the other hand, the actual reduction of spherical symmetry due to distortions of the C_{60} for any reason

implies a breakdown of degeneracies and modification of the subtle details of the quantum nature of the incarcerated H_2. All of the issues described in the previous paragraphs will be discussed in this review.

As discussed above, infrared spectroscopy (IR), inelastic neutron scattering (INS) and nuclear magnetic resonance (NMR) all probe the quantum dynamics of the H_2 inside C_{60} at different energy and time scales according to their specific selection rules. Studies at cryogenic temperatures (temperatures a few degrees from absolute 0 K) allow measurements essentially uncomplicated by significant populations of excited levels and therefore provide a clearer basis for the interpretation of results. IR and INS experiments are sensitive to the energy level structure of the spatial modes of the incarcerated H_2. Variation in the strength of the H–H interaction, in the average bond length via changes in the vibrational frequency and in the rotational constant (as compared to the free H_2), quantization of the translational modes, and translational rotational couplings are *directly* observed in IR and INS spectra. NMR detects only the spin 1 ortho-H_2 isomer since para-H_2 ($I = 0$) is NMR silent. However, NMR can be very sensitive to minute variation of the environment (lattice) of a $H_2@C_{60}$ molecule. Indeed, measurements of spin relaxation rates at cryogenic temperatures, encode information about the local environment and rotational dynamics as sensed by hydrogen with odd rotational quantum numbers j.

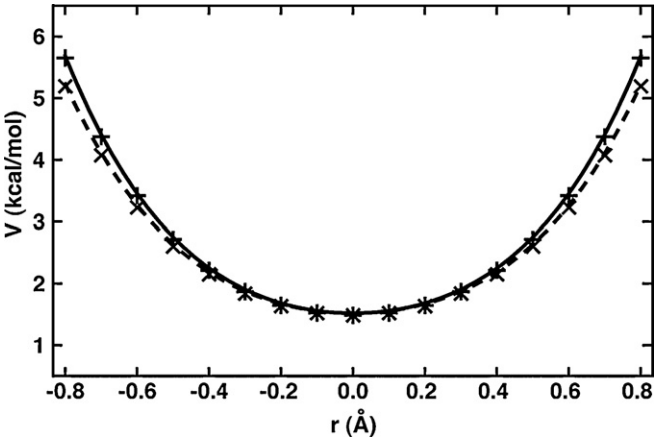

Fig. 2. The effective potential experienced by a hydrogen molecule constrained inside the C_{60} cage as obtained from *ab initio* calculation. Here the centre of H_2 is moved along a C_5 axis joining opposite pentagonal face of the fullerene (x) and perpendicular to it (+) while the H–H bond is kept aligned along the C_5 axis in both cases. The quadratic dependence on the distance from the centre of the fullerene is evident. The difference between the two potential shapes is due to translation–rotation couplings.
Adapted from Ref. [16].

2. Quantum dynamics of $H_2@C_{60}$

The quantum dynamics of H_2 encapsulated in a fullerene depends on the non-covalent (supramolecular) interaction between the two molecules. At a higher order level, the balance between the attractive and repulsive part of the dispersive interaction between H_2 and the carbon atoms of the C_{60} inner wall dictates the effective motion of the two bonded and confined hydrogen nuclei. An interesting question is which model is more realistic in describing $H_2@C_{60}$: a freely rotating H_2 interacting only slightly with the walls of the carbon cage or an H_2 molecule tightly wedged inside the C_{60}? This question was addressed by Cross [16] well in advance of the availability of $H_2@C_{60}$. *Ab initio* computation of the potential electronic surface (PES) at the level of the Hartree-Fock method and the 6-31G(d,p) basis set indicated that H_2 should rotate freely inside the almost isotropic potential generated by C_{60} (Fig. 2). The calculated potential was found, however, to have a small dependence on the H_2 orientation that acts as a torque pushing the hydrogen toward a parallel orientation to the fullerene surface. The parabolic profile of the confining potential suggests the validity of an analysis of the quantum dynamics of $H_2@C_{60}$ in terms of eigenfunctions of a free rotating molecule oscillating in an almost isotropic harmonic potential. More accurate quantum calculations have mainly focused in the evaluation of stabilization energies [17]. To date high-level computations of PES for endohedral fullerene compounds are not available.

Effective potentials are extremely useful, since it is computationally feasible to solve exactly the five dimensional (5D) Schrödinger equation of a rigid hydrogen molecule confined in nanoscopic structures [18]. The difficulty of finding a reliable PES from first principles can be circumvented assuming that the cage–hydrogen interaction can be obtained as a sum of a two-body interaction V_{C-H_2} over all the carbon atoms [19]. A Lennard–Jones (LJ) potential is then used to describe the dispersion interaction between the carbon atom and the hydrogen molecule. The energy level patterns resulting from the translation–rotation coupling which were computed on the PESs constructed using the standard two-site LJ pair potentials [19] were observed in the infrared spectra of $H_2@C_{60}$ [20]. However, the agreement between the calculated and measured excitation energies was not quantitative. On the other hand, a three site potential, which incorporates one additional parameter, has been found to describe the interaction between a carbon atom and the hydrogen molecule much better: the carbon atom interacts with the molecular charge distribution which is located not exclusively at the nuclear positions but also in the intermediate space between the hydrogen atoms. Importantly, this improved potential reproduces accurately the frequencies of six of the observed IR peak positions in ortho-$H_2@C_{60}$ and para-$H_2@C_{60}$ IR spectra [21].

The potential energy surface parameters, spectroscopically optimized for $H_2@C_{60}$, were successfully used to analyze the quantum dynamics of H_2 confined in the anisotropic fullerene C_{70} [21,22]. Not surprisingly, given the weak anisotropy, radial and angular, of the interaction between H_2 and C_{60}, the solutions of the 5D Schrödinger equation, computed from the optimized potential, revealed that a rational interpretation of the $H_2@C_{60}$ dynamics can be understood in terms of a quantum rotor confined in an isotropic harmonic potential, whose eigenstates can be labelled by the set of the quantum numbers $v, j, n, l, \lambda, m_\lambda$ [19,20]. The integer $v = 0, 1, \ldots$ represents the vibrational quantum number. The angular momentum $\boldsymbol{J}$ associated with the rotation of H_2 with respect to its centre of mass is quantized according to $|\boldsymbol{J}| = \sqrt{j(j+1)}\hbar$ with $j = 0, 1, \ldots$. In the absence of a spin catalyst, or higher order interactions of H_2 with the cage which would lower its symmetries [23,24], matrix elements connecting ortho and para states are null, justifying the net separation of the Hamiltonian treatment for the two spin isomers. The quantization of the centre of mass motion is described by the two quantum numbers [25] n, which counts the number of translational excitations 0, 1, ... and l, which expresses the quantization of the H_2 centre of mass angular momentum $|\boldsymbol{L}| = \sqrt{l(l+1)}\hbar$. For a given n, the angular momentum number may assume positive integer values $l = n, n-2\ldots$ until 1 or 0, depending on n being even or odd, respectively. The quantum numbers λ and m_λ are related to the spherical symmetry of the system and define the transformation properties of the combined translation–rotation spatial wave function under rotation. λ is associated with the total angular momentum $\wedge = \boldsymbol{L} + \boldsymbol{J}$ and can assume integer values restricted to $|l-j| \leq \lambda \leq l+j$ and $m_\lambda = -\lambda, \ldots, \lambda$ is the projection along any quantization axis. In a purely harmonic potential the role of λ in labelling energy levels is immaterial. In $H_2@C_{60}$ the small size of the confinement induces translation–rotation couplings that lift the

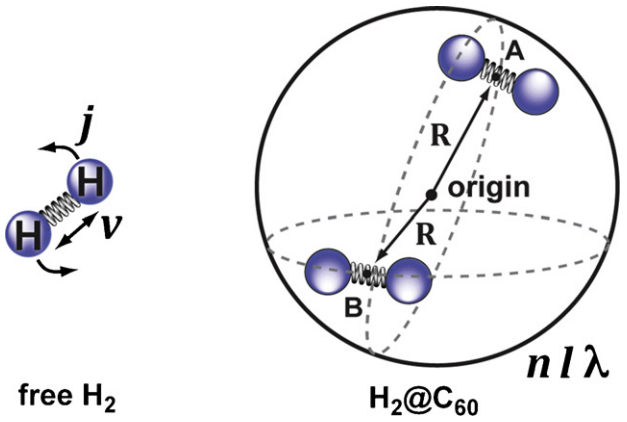

Fig. 3. Confinement of H_2 inside C_{60} introduces new quantum numbers, n, and λ. For free H_2, the quantization of the vibrational v, and rotational, j, degrees of freedom is apparent. Both motions occur with respect to the centre of mass of H_2 (left picture). For confined H_2 (right picture), the translational degrees of freedom are quantized and are described by two additional quantum numbers of the 3D isotropic harmonic oscillator [25]: the number of translational excitations n and the orbital angular momentum quantum number l. n describes the dependence of H_2 *translational* wavefunction on the distance R from the origin of C_{60} and l describes its angular dependence. The two angular momenta, quantum numbers j and l, are coupled to each other: the H_2 has to rotate around its centre of mass (j-motion) while moving along trajectories which pass through A and B (l-motion), resulting in a new quantum number λ[14].

degeneracy of the translational levels. The energy levels in $H_2@C_{60}$ can roughly be obtained from

$$E(v, j, n, \lambda) = \left(v + \frac{1}{2}\right)\omega_v + \left(n + \frac{3}{2}\right)\omega_n + B_v j(j+1) + c(l, j, \lambda)V_{T-R} \quad (1)$$

in units of reduced Planck constant $\hbar$. Here ω_v is the vibrational quantum of energy, ω_n is the translational quantum of energy, $B_v = B_e - \alpha_e(v{+}1/2)$ is the rotational constant in the state v and α_e represents a vibration–rotation correction. The last term is proportional to the translation–rotation coupling V_{T-R} through a coefficient $c(l,j,\lambda)$ that gives the pattern of the sublevels. Such a coefficient depends on the detailed spherical form of the translation–rotation coupling. The degeneracy of the level with a given set of quantum numbers is $g = 2\lambda + 1$. A pictorial representation of the relationships between the quantum numbers and the various degrees of freedom in H_2, and $H_2@C_{60}$ is given in Fig. 3.

The description given above is oversimplified to some extent, but it can be used as a guide in the interpretation of the observed spectra. First, the carbon framework is treated as rigid and non-rotating. This is justified at 4 K as the vibrational frequencies span over the range 260–1575 cm^{-1} [26], well above the k_BT and the rotations of C_{60} are frozen out at temperatures below about 100 K as shown by NMR experiments, see Section 6. Second, realistic confining potentials must include anharmonic terms that imply a non uniform spacing between translational excitations. Third, higher order corrections: vibration–rotation couplings, centrifugal distortion and vibration–translation coupling are not included in Eq. (1). Fourth, the real icosahedral symmetry of C_{60} reduces the $2\lambda + 1$ spherical degeneracy and levels with $\lambda \geq 3$ split in a multiplet according to the irreducible representation of the group I_h [19]. The effect is tiny and the resulting energy gaps in the multiplet are small. Tables 1 and 2 report the energy levels computed via exact numerical solution of the fully coupled 5D Schrödinger equation for the translational and rotational degrees of freedom of para- and ortho-$H_2@C_{60}$ in the first excited vibrational state $v = 1$ using a spectroscopically based three-site potential and the icosahedral symmetry of C_{60} [21].

Table 1
Translation–rotation energy levels of para-$H_2@C_{60}$ in the first excited vibrational level $v = 1$ from the quantum 5D calculations on the IR optimized PES in reference [21]. The excitation energies ΔE in cm^{-1} are relative to the translation rotation para-H_2 ground-state energy in the $v = 1$ state. g is the degeneracy of the level. $\langle R\rangle$ is the mean value of the distance between the centre of mass of H_2 and C_{60} in atomic units. The quantum numbers n, j, λ, l define the state in terms of the harmonic basis as reported in the text. The effect of translation rotation couplings is evident. $c(j)$ is the contribution of the dominant rotational basis function having the quantum number j. The closely spaced levels, whose energies are in italics, arise from the lifting of the $2\lambda + 1$ level degeneracy of the spherical approximation by the icosahedral potential of C_{60}.

	$\Delta E/c$ (cm^{-1})	g	$\langle R\rangle$	n	λ	j	$c(j)$	l
0	0.00	1	0.70	0	0	0	0.999	0
1	183.47	3	0.87	1	0	1	0.999	1
2	328.63	5	0.70	0	2	2	0.993	0
3	382.87	5	0.99	2	0	2	0.991	2
4	409.38	1	0.96	2	0	0	0.997	0
5	507.01	5	0.87	1	2	2	0.999	1
6	*513.40*	4	0.87	1	2	3	0.991	1
7	*513.50*	3	0.87	1	2	3	0.991	1
8	518.22	3	0.87	1	2	1	0.996	1
9	*596.09*	4	0.86	3	0	3	0.988	3
10	*596.92*	3	1.09	3	0	3	0.987	3
11	683.21	3	1.09	3	0	1	0.992	1
12	*705.06*	3	1.05	2	2	3	0.999	2
13	*705.32*	4	1.00	2	2	3	0.999	2
14	707.14	5	0.99	2	2	2	0.999	0,2
15	*713.67*	4	0.99	2	2	4	0.989	2
16	*713.96*	5	0.99	2	2	4	0.988	2
17	717.78	3	0.99	2	2	1	0.999	2
18	724.07	3	0.99	2	2	0	0.993	2
19	741.23	1	0.98	2	2	2	0.994	0,2
20	*822.69*	4	1.17	4	0	4	0.985	4
21	*823.60*	5	1.17	4	0	4	0.985	4
22	879.05	5	1.13	4	0	2	0.986	2
23	902.81	1	1.11	4	0	0	0.987	0

Reprinted with permission from reference [21], Copyright 2009, American Institute of Physics.

Table 2
Translation–rotation energy levels of ortho-$H_2@C_{60}$ in the first excited vibrational level $v = 1$ from the quantum 5D calculations on the IR optimized PES in [21]. The excitation energies ΔE in cm^{-1} are relative to the translation–rotation para-H_2 ground-state energy in $v = 1$ state. The symbols and the meanings of the various entries are the same as in Table 1.

	$\Delta E/c$ (cm^{-1})	g	$\langle R\rangle$	n	λ	j	$c(j)$	l
1	109.63	3	0.70	0	1	1	0.999	0
2	287.72	3	0.87	1	1	1	0.999	1
3	294.23	5	0.87	1	1	2	0.999	1
4	304.55	1	0.86	1	1	0	0.999	1
5	484.48	5	1.00	2	1	2	0.999	2
6	*494.07*	4	0.99	2	1	3	0.998	2
7	*494.58*	3	0.99	2	1	3	0.998	2
8	496.10	3	0.98	2	1	1	0.999	0,2
9	524.21	3	0.95	2	1	1	0.999	0,2
10	*658.16*	4	0.70	0	3	3	0.999	0
11	*658.18*	3	0.70	0	3	3	0.999	0
12	*694.87*	3	1.10	3	1	3	0.999	3
13	*695.58*	4	1.10	3	1	3	0.999	3
14	707.92	4	1.09	3	1	4	0.995	3
15	708.56	5	1.09	3	1	4	0.995	3
16	710.38	5	1.08	3	1	2	0.999	1,3
17	737.80	3	1.05	3	1	1	0.999	1
18	754.49	5	1.04	3	1	2	0.993	1,3
19	770.39	1	1.03	3	1	0	0.998	1
20	*836.04*	3	0.87	1	3	3	0.999	1
21	*836.08*	4	0.87	1	3	3	0.999	1
22	*844.04*	4	0.86	1	3	4	0.996	1
23	*844.19*	5	0.86	1	3	4	0.995	1
24	846.87	5	0.86	1	3	2	0.994	1

Reprinted with permission from reference [21], Copyright 2009, American Institute of Physics.

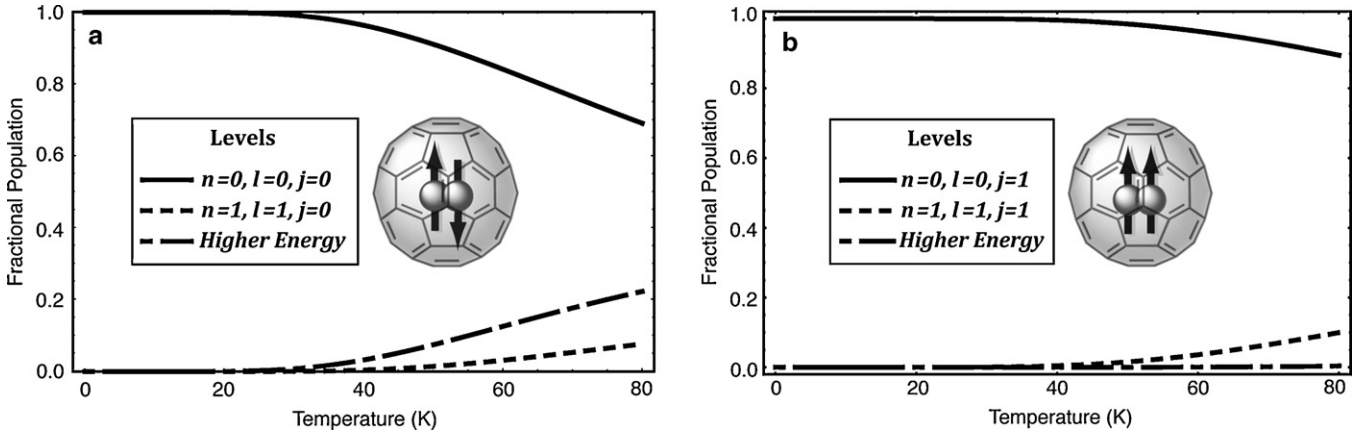

Fig. 4. Temperature dependence of para-H_2@C_{60} and ortho-H_2@C_{60} populations at thermal equilibrium on the left and on the right respectively. At temperatures below 30 K only the ground vibrational–rotational–translational states are populated.

In conclusion, in H_2@C_{60} the encased molecule–cage interaction can be separated into two parts: a "large" spherically symmetric potential and a residual "small" icosahedral potential. Experimental and theoretical calculations, reported in this review, prove that the dynamics of the endohedral hydrogen is mainly determined by the spherical part of the potential. The coupling between the motion of the endohedral molecule and the rotation of the cage is weak because of the small icosahedral part of the potential compared to the distance between the translation and rotation levels of H_2. The interpretation of the levels of the endohedral hydrogen in terms of the quantum numbers of the free rotor coupled to harmonic oscillator and the effect of symmetry reduction are evident.

3. Populations of the energy levels of ortho-H_2 and para-H_2 at thermal equilibrium

Ortho-H_2 and para-H_2 are metastable allotropes of molecular hydrogen with rates of interconversion that are extremely slow in the absence of a spin catalyst. In the (hypothetical) absence of external catalysts, H_2@C_{60} spin conversion could still occur because of mixing with excited electronic states or because of interactions that result in small differences in local magnetic fields at the two proton positions. One such mechanism might involve interactions with natural-abundance ^{13}C nuclei in the cage (about 48% of C_{60} molecules contain at least one ^{13}C nucleus). Nevertheless, both mechanisms lead to such low rates that essentially no interconversion for H_2@C_{60} has been unambiguously observed in any experiment so far in the absence of a deliberately added spin catalyst. After its preparation, H_2@C_{60} near room temperature contains molecular hydrogen spin isomers in a ratio that is determined by the initial balance of H_2 allotropes when the complex is prepared. Since the hydrogen capture step in the synthesis is performed at room temperature or above, the normal ortho to para ratio of encapsulated H_2 molecules is 3:1, although methods for enrichment of para- H_2@C_{60} have been recently devised [27,28]. Once H_2@C_{60} is prepared with a fixed ortho to para ratio the two isomers act as independent thermal reservoirs. At a given temperature the fast thermalization of the non-nuclear spin degrees of freedom in molecular hydrogen ensures that the quantum levels are populated according to the Boltzmann distribution of each of the two allotropic species, but the two allotropes do not equilibrate with each other. Fig. 4 describes the equilibrium para-H_2 and ortho-H_2 fractional population of the energy levels for temperatures below 80 K as obtained from the energies and degeneracies in Tables 1 and 2. There is a subtlety here because the energies of the spatial eigenfunctions are calculated for the first excited vibrational state $v = 1$. It is supposed that the differences with the correspondent energies for the ground vibrational state $v = 0$ are small. Indeed, the plotted distributions are insensitive to the fine details in the energy level positions. They are related to the large translational and rotational energy gaps compared to the thermal energy k_BT. It is evident that only the vibrational–rotational–translational ground states are populated below 30 K.

The temperature effect upon spectroscopy is threefold. First, spectra at low temperatures are less congested because only the ground ortho-H_2 and para-H_2 states are macroscopically populated: the observed transitions involve only the ground state levels as initial states. Second, for the same reason the intensity of the lines is higher, resulting in enhanced spectroscopic sensitivity. Third, the rotational dynamics of the cage is frozen, as described in the NMR Section 6, allowing interpretation of the experiments in terms of modes of H_2 in a fixed geometry.

4. IR spectroscopy of H_2@C_{60} at low temperatures

The IR spectroscopy of H_2@C_{60} at temperatures near 4 K clearly shows the fingerprints of the quantization of the H_2 spatial degrees of freedom. The IR absorption peaks of H_2@C_{60} at 6 K are located in 4 narrow regions between 4060 and 4800 cm^{-1} as shown in Fig. 5. The observed lines can be described as combination of the forbidden vibration band, $\Delta v = 1$, with the IR allowed translation mode. At first sight it may be surprising that a homonuclear diatomic molecule like hydrogen is IR active at all. However, the interactions of H_2 with atom or molecules can produce small distortions of the molecular charge distribution so inducing a small dipole moment. For example, IR spectroscopy of H_2 in the condensed phase [29] and intercalated in the voids among the cages in crystalline C_{60} [30–32] has been reported. In a qualitative picture for H_2@C_{60}, the carbon π orbitals push the hydrogen electronic cloud to the centre of the C_{60} cage, while nuclei move back and forth so creating a dipole moment modulated by the nuclear motion. The instantaneous dipole moment is a function of the hydrogen configuration coordinates inside C_{60}. The rigorous treatment requires *ab initio* evaluation of three main induction mechanisms [33]; dispersion, electron exchange, and electric multipolar, in a similar way to that done for H_2-noble gas systems [34,35]. A quantitative analysis of the H_2 induced IR activity can be performed by expanding the dipole moment in terms of appropriate spherical multipoles [32,36]. The selection rules for IR spectroscopy on H_2@C_{60} follow from the vectorial nature of the dipole moment. They are clearly expressed in the coupled spherical basis defined by the l, j, λ quan-

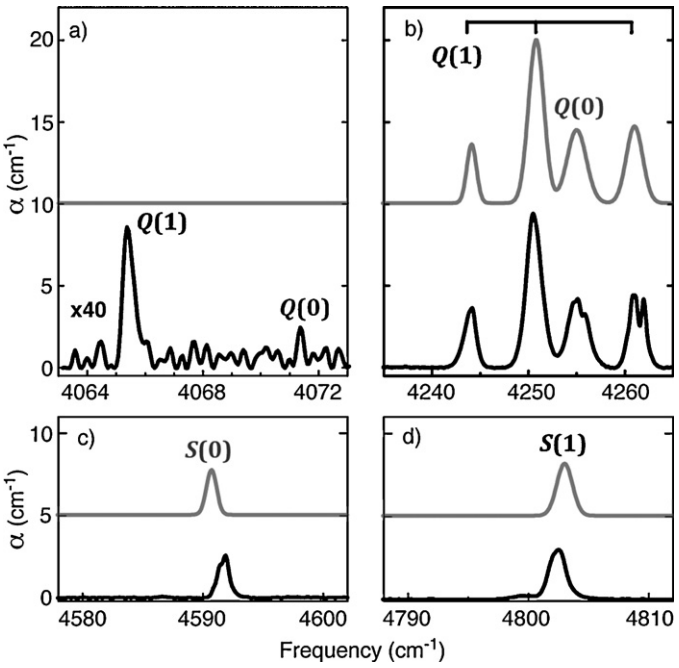

Fig. 5. IR spectra of $H_2@C_{60}$ at 6 K. The four panels show the experimental spectra (in black) and the simulated ones in the harmonic confined vibrating rotor approximation (in gray and located directly above the experimental spectra). The label over the lines represents the spectroscopic notation for vibrational bands: the capital letters denote the variation in the rotational quantum number between the initial and final states, with Q and S indicating $\Delta j = 0$ and $\Delta j = 2$, respectively. The numbers in the round parentheses represent the j value in the initial state.
Adapted from Ref. [20].

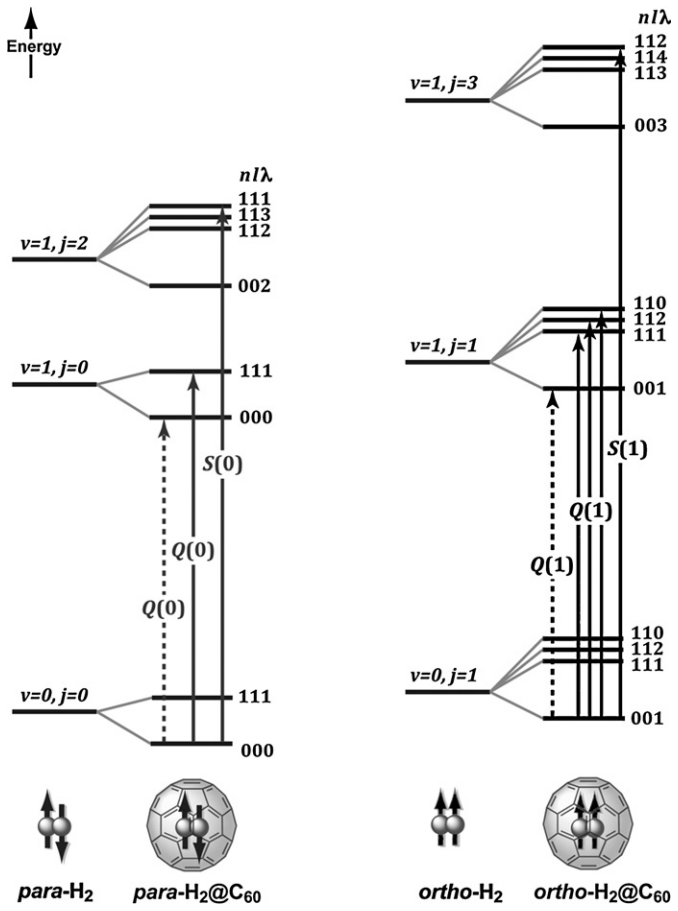

Fig. 6. Diagrammatic scheme showing the transitions and the corresponding energy levels that are relevant for IR spectroscopy on $H_2@C_{60}$ at temperature near 4 K: para-H_2 is on the left and ortho-H_2 is on the right. The transitions on the left energy diagram corresponds to the para component and the transitions on the right energy diagram corresponds to the ortho component. The dotted lines stand for forbidden transitions in the isolated $H_2@C_{60}$. Infrared spectroscopy at cryogenic temperatures involves transitions from the ground state to the first excited vibrational manifold. The effect of confinement in C_{60} is to split the vibrational–rotational energy manifold of free H_2 in translational sublevels labelled by the set of quantum numbers n, l, λ as discussed in the text. In the ground $v = 0$ state the $j = 2$ and $j = 3$ energy levels are not shown.

tum numbers: $\Delta\lambda = 0, \pm 1$ (angular momentum conservation), $|\Delta j|$ even and $|\Delta l|$ odd (inversion symmetry) [20]. Diagonalization of a vibration–rotation and translation Hamiltonian in the presence of perturbing translation–rotation coupling together with intensity analysis based on an effective expansion of the dipole moment allows one to compute the precise energy levels and to assign the observed transitions [20], as shown in Fig. 6. Note that *IR photons do not excite transitions between the ortho-H_2 and para-H_2 manifolds:* the electromagnetic wave does not couple singlet and triplet nuclear spin states.

The IR transitions shown in Fig. 6 all originate in the lowest energy state of each of the two allotropes, since at 6 K none of the higher states are significantly occupied. The two "weak" lines in panel (a) of Fig. 5 represent the pure H–H stretching $v = 0 \rightarrow v = 1$ transition for para-H_2 (4071 cm^{-1}) and ortho-H_2 (4065 cm^{-1}). The separation between these two lines originates from vibration–rotation couplings, since the two species correspond to different values of j. The fundamental vibrational frequency in both allotropes is redshifted with respect to the gas phase by 90 cm^{-1} implying that the effective hydrogen-fullerene potential is attractive at the centre of the cage [37] making an effective spring connecting the two protons softer. The IR activity of the pure vibrational mode is a result of medium-induced symmetry breaking effects, in this case in the solid state. Group theory arguments imply that no pure vibrational transitions are allowed within the electric dipole approximation by any of the induction mechanisms for isolated $H_2@C_{60}$ even considering the real icosahedral symmetry of $H_2@C_{60}$. The next set of four lines between 4240 and 4261 cm^{-1}, reported in panel (b), represents a pure translational sideband: a translational quantum is excited beside the vibrational one. The fundamental translational excitation in the excited vibrational state is then approximately 184 cm^{-1} (22.8 meV). The Q(0) line corresponds to a para transition while the three Q(1) lines correspond to ortho transitions. The splittings in the Q(1) line are a direct evidence of translation–rotation coupling. In the presence of translational rotational couplings, the energy level with $n = 1$, $l = 1$, $j = 1$ is split in three levels with $\lambda = 1, 2, 0$ which are terminal states for allowed IR transitions from the ground state according to the selection rules stated above. The ordering of the levels depends on the specific form and on the sign of the translation–rotation coupling term [20]. Finally the two panels (c and d) show para and ortho S lines where two rotational quanta are excited beside the translational and vibrational ones. The separation from the Q lines in panel (b) is approximately defined by the value of the rotational constant B_1 according to Eq. (1): the para line S(0) is $6B_1$ and the ortho one is $10B_1$ higher in frequency than the Q lines. The rotational constant of H_2 is reduced to $B_e = 59.3$ cm^{-1}, with $\alpha_e = 2.98$ cm^{-1} [20] compared to the gas phase values $B_e^g = 60.85$ cm^{-1} and $\alpha_e^g = 2.99$ cm^{-1} [38]. This corresponds to a 1.3% increase in the proton–proton distance. The remaining shifts, 8 cm^{-1} for the S(0) line and 4 cm^{-1} for the S(1) line, come from the translation–rotation term $c(l, j, \lambda)$ in Eq. (1) which affects differently the final rotational states that have $l = 1, j = 2, \lambda = 1$ and $l = 1, j = 3, \lambda = 2$, respectively.

The IR spectroscopy of $H_2@C_{60}$ provides direct access to the host-cage potential and molecular parameters. Lines are narrow

because of the homogeneous distribution of the confinement potential and H_2 molecules are isolated from each other by C_{60} molecules. Translational excitation energy, translation–rotation coupling, internuclear distance and vibrational strength can be directly extracted from the analysis of the low temperature IR spectra. High resolution spectra were a stimulus to improve the C–H_2 pair interaction as discussed above for the theory of the H_2@C_{60} system. Finally, the ortho to para ratio can be estimated directly by comparing the observed line intensities with the theoretically predicted ones. In conclusion, quantum theory of H_2@C_{60} provides an excellent framework for the interpretation of the infrared spectrum of H_2 incarcerated in the C_{60} host. The distinct, non-interconverting nature of para-H_2 and ortho-H_2 are directly and clearly demonstrated by analysis of the spectra, as are the coupling of quantized translation and rotation degrees of freedom.

5. Inelastic neutron scattering of H_2@C_{60} at low temperatures

Neutron scattering does not involve electromagnetic interactions with matter. Rather it relies on the nuclear interaction between a beam of neutrons and the nuclei in the molecules that causes transitions between molecular energy levels. Inelastic neutron scattering (INS) experiments involve detecting variations in the energy *and* momentum of the neutron beam when it interacts with the sample. Intensity plots of the scattered neutrons *versus* neutron energy absorbed or neutron energy gained resemble typical electromagnetic spectra linking quantum states of the system under study (Fig. 7). Indeed, the signals produced in INS spectra correspond to the energy level difference between two quantum states, as in all forms of molecular spectroscopy. The INS spectra show energy loss signals corresponding to transitions where neutrons are slowed down and lose energy by transfer to the H_2 system and energy gain signals corresponding to processes in which the H_2 molecules give up some energy to the scattered neutrons. Due to the weakness of the effective neutron interaction with nuclei in scattering processes, INS is a relatively insensitive technique requiring a relatively large amount of H_2@C_{60} (~100 mg or more) compared to the amount needed for IR and NMR that give acceptable signals even with few mg of material.

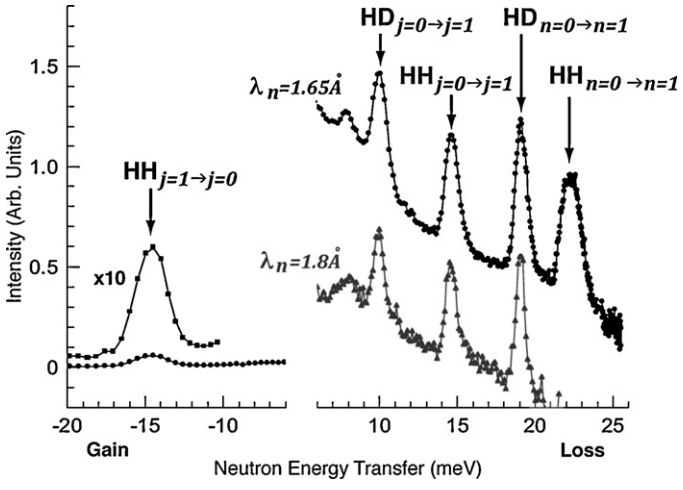

Fig. 7. Inelastic neutron scattering spectra of a H_2@C_{60}:HD@C_{60}:D_2@C_{60} mixture with relative ratio 1:1:0.2 at 1.8 K as obtained with IN4 time of flight spectrometer at ILL facility in Grenoble, France. Energy loss indicates that the energy is transferred from the neutrons to the H_2@C_{60} system and energy gain indicates that energy is transferred in the opposite direction during the scattering process. The offset bottom line in the energy loss section represent INS spectra obtained using incoming neutrons with an energy appropriate to optimize the resolution around 15 meV. Adapted from Ref. [40].

Fig. 7 shows the INS spectra, recorded at 1.8 K, of a mixture of the hydrogen isotopomers H_2@C_{60}:HD@C_{60}:D_2@C_{60} with relative ratio 1:1:0.2. Analogous to the "absorbance" or the "extinction coefficient" of a material in electromagnetic interactions which represent cross-sections for the interactions of the electrons and atoms of a molecule with electromagnetic radiation, the "intensity" of the INS spectrum is determined by coherent and incoherent scattering cross-sections. The neutron–nucleus interaction has a spin-dependent term, sensitive to the relative orientations of the neutron and nuclear spins: the scattering from a lattice will vary from one lattice site to another due to differences in orientation of the nuclear spins and isotopic composition [39]. Coherent scattering arises from the average scattering potential whereas incoherent scattering represents the deviations from the average scattering potential. Coherent scattering can give rise to interference effects and is important in neutron diffraction. However, to elucidate the molecular dynamics where the motion induces its own fluctuations on the lattice of scattering sites, the incoherent scattering is the important component. Since they are a property of nuclear physics, the cross-sections naturally depend sensitively on the isotopic species. However, there is no systematic variation in scattering cross-section with atomic number or mass number. Importantly, the ^{1}H *incoherent* cross-section is much larger than the ^{1}H coherent cross-section and also is much greater than the combined ^{2}H, ^{12}C and ^{13}C coherent and incoherent cross-sections. As a result, INS spectra of H_2@fullerenes are dominated by incoherent scattering from ^{1}H. Therefore, all of the carbon atoms of the C_{60} cage are essentially "invisible" to the neutron beams and do not produce a measurable signal.

A wide range of energy transfers, and therefore transitions between energy levels, can be probed by INS, depending on the configuration of a particular spectrometer. On the IN4 time-of-flight spectrometer used to record the spectra in Fig. 7 the energy transfer is in the range of ~10 meV (~80 cm^{-1}). Such values match rotational–translational transitions in the *ground* vibrational state of H_2 and HD.

The absence of ortho/para isomers for heteronuclear diatomic molecules, such as HD, implies a much stronger temperature dependence of the peak intensities for HD@C_{60} than H_2@C_{60} since the rotational states of HD are not locked in the stringent selection rules that H_2 must obey because of the Pauli principle. Therefore at sufficiently low temperatures only the lowest energy state of HD is occupied. This distinct characteristic between H_2 and HD would be revealed by a comparative analysis of the temperature dependence of the INS of H_2@C_{60} and HD@C_{60}. Indeed, a variable temperature analysis of the INS data allows one to clearly distinguish among H_2 and HD transitions [40]. The observed INS transitions for H_2 at low temperatures are shown by the arrows in the rotational energy level diagram (Fig. 8).

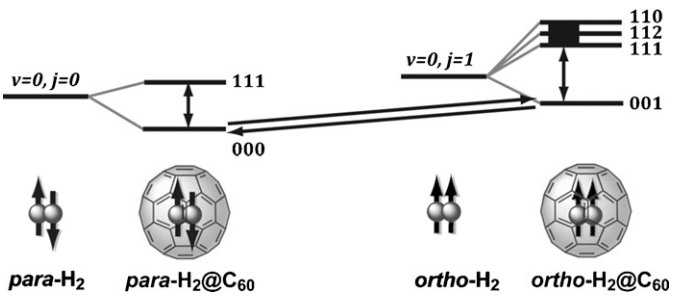

Fig. 8. Diagrammatic scheme showing the transitions and the corresponding energy levels that are relevant for INS experiments on H_2@C_{60} at temperature near 4 K: para-H_2 is on the left and ortho-H_2 is on the right. In the energy range of ~10 meV, INS experiments at cryogenic temperatures probe transitions only in the ground vibrational state $v = 0$.

One of the most relevant features of the neutron interaction with matter is the explicit spin dependence. Transitions connecting ortho-H_2 to para-H_2 states and vice versa are observable in INS, since the neutron carries spin that allows the spin conservation requirements to be obeyed. The peak (Fig. 7, $HH_{j=0\rightarrow j=1}$) at 14.6 meV (117.8 cm^{-1}) in neutron energy loss corresponds to the pure rotational transition, $\Delta\lambda = +1$, from the para ground state to the ortho ground state. In free H_2 this highly forbidden transition in IR spectroscopy is at 118.6 cm^{-1}. The associated peak in neutron energy *gain* corresponds to the reverse transition from ortho to para. Differences in intensity reflect the relative proportions of ortho- and para-H_2. The difference in width of corresponding energy gain and loss peaks is a function of the spectrometer resolution and is not intrinsic to the sample. From IR analysis a ground state splitting of 115.6 cm^{-1} can be obtained.

It is important to note that the ground state of ortho-H_2 state is triply degenerate ($2\lambda + 1 = 3$), if it exists in a perfectly symmetrical environment, to which the icosahedral environment of C_{60} closely approximates. The corresponding INS transition in an asymmetric open cage fullerene, H_2@ATOCF, while essentially coinciding with that in $H_2@C_{60}$, is split into three peaks [41], proving that the rotational constant (given by the transition energy between the rotational energy levels) is not affected significantly by confinement in a closed fullerene. In addition, the level splitting shows that for H_2@ATOCF the asymmetric molecular field from the cage is able to lift completely the threefold degeneracy among the rotational sublevels in the ortho-H_2 ground state.

In INS, as in other forms of spectroscopy, there is a trade-off between sensitivity and resolution and to date the experiments performed on the IN4 spectrometer at Grenoble have provided no clear evidence of any structure in the analogous $H_2@C_{60}$ rotational peaks. Nevertheless, the resolution limit allows the establishment of an upper limit of 0.3 meV (≈2.4 cm^{-1} or ≈3.5 K) on the size of any ortho-H_2 ground state energy splitting. Such a limit would not allow resolution of a feature observed at 0.1–0.2 meV in specific heat measurements [42] of $H_2@C_{60}$ ascribed to a lowering of the local symmetry of the cage in the solid state. It is also barely within the range of symmetry reduction suggested by the observation of residual anisotropic H–H dipolar coupling in the ^1H nuclear magnetic resonance line shape at 4 K (see Section 6).

The observation of a detectable neutron energy gain peak at −14.6 meV in $H_2@C_{60}$ (Fig. 7, $HH_{j=1\rightarrow j=0}$) strikingly demonstrates the remarkable independence of the two spin isomers, since at 1.8 K thermodynamic equilibrium would imply that all the particles would be in the lowest energy para configuration. For example the neutron rotational energy loss peak corresponding to the pure rotational transition at 10.0 meV in Fig. 7 ($HD_{j=0\rightarrow j=1}$) has no corresponding peak in energy loss at this temperature, since there are no spin symmetry constraints for transitions between all of the rotational levels of HD@C_{60}. In terms of dynamics, the rates of transitions between the $j = 0$ and $j = 1$ (no ortho-para states) rotational levels of HD are of the order of 10^6 s^{-1}, whereas the corresponding rate of transitions between the $j = 0$ and $j = 1$ (para ↔ ortho) rotational levels of H_2 are of the order of 10^{-12} s^{-1}! This difference of more than 18 orders of magnitude between two formally similar rotational transitions is profound and demonstrates the deep power of the Pauli principle to control the dynamics of molecular processes.

The +22.3 meV peak (179.9 cm^{-1}) corresponds to a pure H_2 *translational* transition (Fig. 7, $HH_{n=0\rightarrow n=1}$). The translational excitation energy is similar to that of the first vibrational state $v = 1$ where it is 183.6 cm^{-1} given by difference of the two Q(0) lines of 4255.0 and 4071.4 cm^{-1}, respectively (Fig. 5a and b). This raises another interesting feature of INS connected with the quantum nature of H_2 where the ^1H nuclei appear as a discrete scattering object to the incident neutron. Since para-H_2 has total nuclear spin $I = 0$, there is no inelastic intensity associated with para–para transitions. Only the translational transitions of ortho-H_2 which has $I = 1$ appear in the INS spectrum. By contrast, there are no such constraints for HD, and both $j = 0$ and $j = 1$ species ($I = 1/2$ for hydrogen) can contribute to the purely translational transitions in the INS spectrum.

Surprisingly the translation–rotation splitting seems to be smaller than that expected from the IR observation of the corresponding transitions in the first vibrational state. A detailed discussion of the INS experiments and assignments for $H_2@C_{60}$ can be found in Ref. [40].

In conclusion, at temperatures near 4 K, the interpretation of the INS spectrum of $H_2@C_{60}$ is consistent and complementary to the IR spectroscopy of $H_2@C_{60}$ and the two methods provide essentially identical energy level diagrams. However, INS additionally provides information concerning the transitions between ortho- and para-H_2 manifolds which cannot be observed in IR. The profound difference between H_2 and HD resulting from the Pauli principle is beautifully revealed by the temperature dependence of the INS for the two isotopomers H_2 and HD. The H_2 system shows scattering from both the ortho-H_2 and para-H_2 even at temperatures near 4 K because the Pauli spin isomers cannot interconvert due to the lack of a spin catalyst and the ortho-H_2 population at room temperature persists at 4 K. On the other hand, HD shows scattering only for the lowest rotational level at temperatures near 4 K since only this rotational state is populated.

6. Nuclear magnetic resonance of $H_2@C_{60}$ at low temperatures

Nuclear magnetic resonance (NMR) studies yield a wealth of structural and dynamical information for a wide range of molecular structures. High resolution solution NMR has proved to be a valuable tool for monitoring the interconversion of the ortho (NMR active) and para (NMR silent) allotropes of $H_2@C_{60}$ and related fullerenes [27,28,43]. However, spatial information may be extracted only indirectly from solution NMR spectra via relaxation time measurements, and even then spatial information is often mixed with dynamical effects which are difficult to evaluate [44–47]. Some of the limitations of solution NMR can be overcome to a considerable extent when spectra are obtained from solid samples at low temperatures.

Samples are usually in the solid phase at cryogenic temperatures (a few degrees above 0 K). Solid state NMR (ssNMR) can access a wide range of temperatures from well above room temperature to the mK regime. Indeed, ssNMR has been employed to investigate $H_2@C_{60}$ at temperatures down to a few K [48,49]. Previous NMR studies on interstitial H_2 molecules in solid fullerene C_{60} molecules [50,51] provide a sound framework for analyzing the behaviour of confined H_2 quantum rotors using solid state NMR. The technique has been employed to investigate the timescale and anisotropy of quantum rotation in $H_2@C_{60}$, as well as the behaviour of the cages themselves and the interactions between ortho-hydrogen molecules enclosed in neighbouring cages. In addition, ^{13}C NMR yields information about the dynamics of the C_{60} cages while ^1H NMR can probe directly ortho-hydrogen (recall that para-hydrogen is *not* NMR active).

The solid-state ^{13}C NMR of $H_2@C_{60}$ exhibits clear signatures of temperature-dependent motional phase transitions [48]. Above 240 K, the fullerene cages undergo rapid cage rotations. Below 240 K, free tumbling is replaced by thermally activated jumps among equivalent configurations. Owing to the rapid reorientation of the C_{60} and to the equivalence of the positions of the atoms in the cage, a single narrow ^{13}C peak is observed at temperatures down to 130 K. However, below 130 K, a chemical shift anisotropy (CSA) broadened component appears. Freezing of the rotational motion of the C_{60} cage (on the NMR timescale) is achieved at 100 K, when the

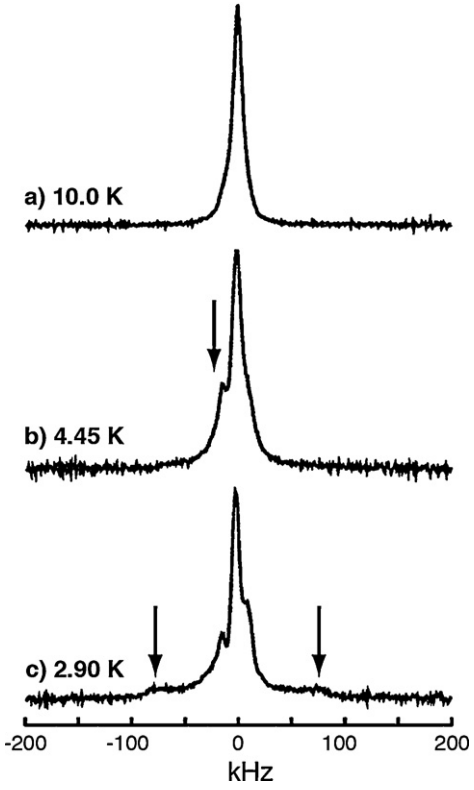

Fig. 9. ^{1}H NMR spectrum of H_2@C_{60} at temperatures of 10.0 K, 4.45 K and 2.90 K in a magnetic field of 8.5 T (360 MHz proton Larmor frequency). Adapted from reference [49].

sharp component vanishes: the static spectrum consists entirely of a CSA broadened peak. The cage dynamics in H_2@C_{60} is very similar to that in pure C_{60}, although the motional transitions in C_{60} are observed at a temperature ≈20–40 K higher than in H_2@C_{60} [52].

The ^{1}H NMR spectra of H_2@C_{60} at 10 K, 4.45 K and 2.90 K are shown in Fig. 9 [49]. In this relatively small temperature range the line shape is visibly modified with respect to higher temperatures [49]. In the large temperature window from room temperature down to 10 K the spectrum (Fig. 9a) consists of a single narrow (≈1 kHz) component with a characteristic chemical shift of −1.1 ppm: since the hydrogen molecule inside C_{60} has free isotropic rotational freedom, the anisotropic interactions are nearly averaged out [49]. However, the width of the signal gets broader at lower temperature when motional averaging among the three sub-rotational ortho-H_2 ($\lambda = 1, m_\lambda = 1, 0, 1$) levels becomes less effective.

At 4.45 K some interesting features appear at the sides of the central peak (Fig. 9b, arrow) [49]. So far, these features are unexplained although they may hint at spin-rotation effects related to rotational molecular resonance effects observed in molecular beam experiments [53,54].

As the temperature is lowered to 2.90 K in addition to the sharp feature, a weak broad feature (≈170 kHz) appears at the base of the main sharp peak (Fig. 9c, arrows). Such a broad feature is consistent with a homonuclear dipolar powder pattern ("Pake pattern") as observed in interstitial H_2@C_{60} complexes [51] and H_2 trapped in asymmetric cages [48]. The peak-to-peak separation (distance between the arrows in Fig. 9) in the "Pake pattern" is consistent with a homonuclear dipolar coupling of ∼116 kHz. This corresponds well to the theoretical dipolar coupling in the $j = 1$ rotational state. The delocalization of the $j = 1$ quantum wavefunction leads to a scaling of the dipolar interaction by a factor 2/5 when compared to the interaction between localized hydrogen at the same internuclear distance [55].

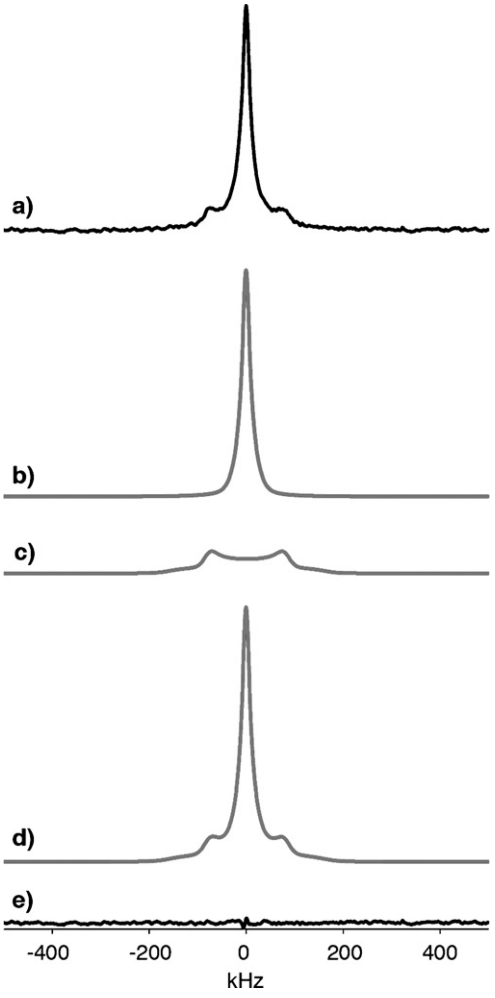

Fig. 10. ^{1}H NMR spectrum of H_2@C_{60} obtained at a temperature of 4.8 K in a magnetic field of 14.1 T (600 MHz proton Larmor frequency). (A) "Solomon echo" $90_x-\tau-90_y-\tau$–acquire sequence was used with additional phase cycling to reduce experimental artefacts. The delay τ was 200 μs and the 90° pulse duration was 2.1 μs. (b) Simulated narrow component (with a Lorentzian/Gaussian mixed peak-shape); (c) simulated Pake-pattern broad component; (d) superposition of the simulated components; (e) residual demonstrating the good match to the experimental lineshape. The ratio of the integrated components is 1.87:1 (narrow:broad).

The low temperature Pake pattern is shown more clearly in Fig. 10. This shows new spectral data obtained on a purified and highly crystalline sample of H_2@C_{60} at 4.8 K, using a "Solomon echo" sequence [56] to avoid interference from acoustic ringing and from probe background signals. The spectrum displays two distinct components: a narrow central peak and a broad component which has the "Pake pattern" form.

The presence of Pake-pattern features in the low temperature ^{1}H spectra indicates that the local H_2 environment does not possess exact cubic symmetry, at least in part of the sample. The reduced symmetry of the H_2 sites causes a splitting of the rotational m_λ levels. The temperature at which these effects are observable in H_2@C_{60} implies rotational splitting of order of few Kelvin ($1\,K = 1.44\,cm^{-1}$), a result which is consistent with specific heat measurements [42]. The observed symmetry reduction may be related to statistical disorder caused by impurities, natural ^{13}C nuclei, cages containing ortho-H_2 and para-H_2 molecules or empty cages. Symmetry reduction may be also an intrinsic feature of the molecular organization in C_{60} crystals, which adopt the simple cubic structure at low temperatures [57]. At the present the mechanism of the observed symmetry reduction is not known.

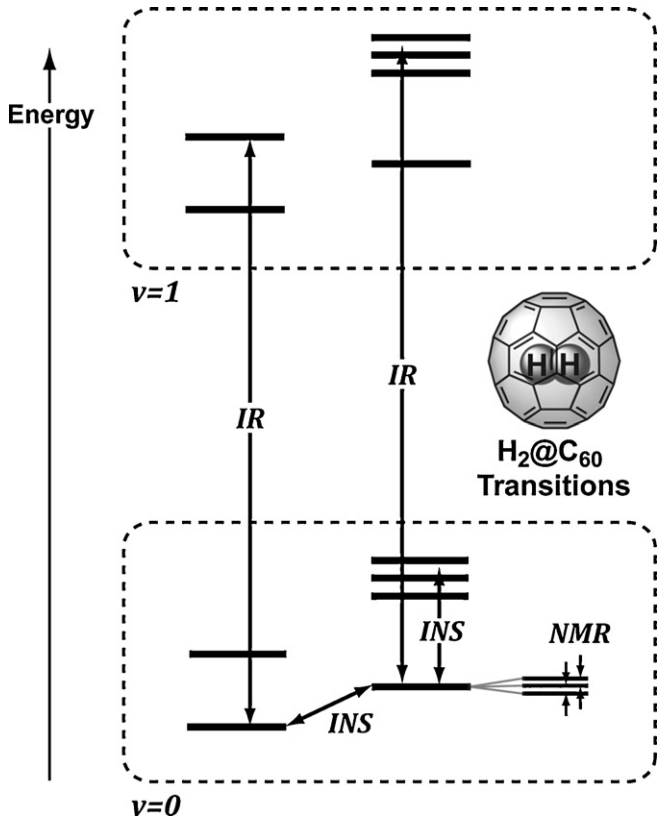

Fig. 11. Summary of the key energy levels of $H_2@C_{60}$ described in this review. (a) IR spectroscopy at crogenic temperatures detects transitions between vibrational levels separated by $\sim 4000\,cm^{-1}$. There are no transitions between the ortho and para spin isomers. (b) INS at at cryogenic temperatures detects transitions between rotational levels. Transitions between ortho and para spin isomers are allowed. (c) NMR at cryogenic temperatures detects very low-energy magnetic dipole transitions of the ortho-hydrogen rotational and translational ground state. The configuration of the orthohydrogen ground state energy sublevels is currently not known (see text).

Interactions between H_2 molecules in adjacent C_{60} cages may also play a role in the dynamics of H_2 at temperatures below 10 K. Indeed, at high temperatures the nature of the coupled ^1H network has been analyzed by using NMR recoupling techniques [41] which show that H_2 molecules are part of a multi-spin system. The existence of such a network implies the possibility of concerted H_2 motion and the fascinating hypothesis of the onset of quadrupolar order [58] in $H_2@C_{60}$ at very low temperatures.

In the case of H_2 trapped inside an asymmetric open-cage fullerene, a full and consistent interpretation of the NMR results is available [48]. Unfortunately this favourable situation does not yet exist for the symmetric $H_2@C_{60}$ system. The low-temperature NMR spectra are fully consistent neither with the theoretical expectations for the case of an undistorted icosahedral cage, nor with that expected for the split energy-level structure evidenced by heat capacity measurements. Further work is in progress on this problem.

7. Conclusions

The energy level diagram in Fig. 11 provides an overview of the quantum transitions studied by IR, INS, and NMR spectroscopy. This shows how these three different physical techniques complement each other in providing a full picture of the quantum dynamics in this physical system.

The $H_2@C_{60}$ molecule and other related endofullerenes provide a fascinating supramolecular complex for the exploration of the quantum characteristics of a rotor trapped in a nearly spherical host. The system is unique in its accessibility to precise theoretical computations that can be compared to spectroscopic techniques such as IR, INS and NMR at temperatures near 4 K. The quantization of H_2 translational motions and the coupling of translational and rotational motions are predicted by theory and clearly demonstrated by IR and INS investigations. The operation of the Pauli principle and its requirement for the entanglement of the rotational and nuclear spin states is beautifully revealed by the IR and INS studies. The subtleties of the environment (inhomogeneities in the lattice due to the existence of ortho-H_2 and para-H2 or adventitious impurities that distort the lattice) can be revealed by ssNMR analysis at cryogenic temperatures. Future IR, INS and NMR experiments, together with theory, promise further refinements of the quantum secrets of the marriage of the simplest molecule, H_2 and one of the most symmetrical molecules, C_{60}.

8. A coda

A coordination chemist who has gotten this far into this review is certainly entitled to ask "What is a review of the spectroscopy of $H_2@C_{60}$ doing in CCR"? First, since this issue is a tribute to Harry Gray, my colleague of nearly 5 decades, the article is a celebration of the ability of this great scientist to see, because of his outstanding scholarship and knowledge and respect for past science, what others before him have missed in some cases.

So let us digress briefly to describe how we might take a cue from Harry and find a reasonable justification for the appropriateness of including this article in Coordination Chemistry Reviews. Certainly any article derived from the teachings of Alfred Werner would be an appropriate candidate for publication in Coordination Chemistry Reviews.

Alfred Werner was awarded the Nobel Prize in Chemistry in 1913 "In recognition of his work on the linkage of atoms in molecules by which he has thrown new light on earlier investigations and opened up new fields of research, especially Inorganic Chemistry".

In his award address Werner states: "I wish to discuss briefly the nature of the affinity forces bringing about the formation of these compounds. I have called these affinity forces secondary valences, to distinguish them from those called primary valences which bring about the formation of first-order compounds. In spite of the vast amount of experimental data we are not yet able to characterize precisely the difference that exists between the two types of valence. Most recent investigations have however shown that there is no fundamental difference between primary and secondary valences and that both types of valence have entirely the same significance for the cohesion of the atoms in the molecule." These "secondary valences" sure sound a lot like the stuff of supramolecular chemistry.

As Lehn [59] has pointed out, novelty in science is rare and often what appears to be novel is simply a new way of looking at past science. Coordination implies the fixation of a selective neighborhood relationship between a host and a guest, i.e., a guest@host complex. In the most general sense from the viewpoint of a guest, coordination means that the host can always be assured to be in its neighborhood of the guest! In this sense, supramolecular chemistry is simply a generalization of Werner's coordination chemistry. The structure of the supramolecular complex, $H_2@C_{60}$, certainly looks nothing like a metal coordination complex to an inorganic chemist. For $H_2@C_{60}$, if you know you are in the vicinity of a H_2 molecule, then you know there are 60 carbon atoms in the neighborhood! The specific structure corresponds to an "endo" coordination, rather than the typical "exo" coordination characteristic of metal complexes.

This perhaps more liberal view of coordination is not particularly revolutionary if we ignore theories of bonding at the first level and just think about neighborhood relationships that are determined by experiments. Once the neighborhood has been established, an appropriate theory will follow!

Acknowledgements

The authors thank the NSF for generous support of this research through grant number CHE 07 17518, the Estonian Ministry of Education and Research Target Financing Grant No. SF06900s09, and the Engineering and Physical Sciences Research Council of the UK.

References

[1] http://nobelprize.org/nobel_prizes/physics/laureates/1932/, in: "The Nobel Prize in Physics 1932" Nobelprize.org.
[2] A. Farkas, Orthohydrogen Parahydrogen and Heavy Hydrogen, University Press, Cambridge, UK, 1935.
[3] M. Saunders, H.A. Jiménez-Vázquez, R.J. Cross, S. Mroczkowski, D.I. Freedberg, F.A.L. Anet, Nature 367 (1994) 256–258.
[4] M. Saunders, H.a. Jimenez-Vazquez, R.J. Cross, S. Mroczkowski, M.L. Gross, D.E. Giblin, R.J. Poreda, J. Am. Chem. Soc. 116 (1994) 2193–2194.
[5] M. Saunders, R.J. Cross, H.A. Jimenez-Vazquez, R. Shimshi, A. Khong, Science 271 (1996) 1693–1697.
[6] K. Yamamoto, M. Saunders, A. Khong, R.J. Cross, M. Grayson, M.L. Gross, A.F. Benedetto, R.B. Weisman, J. Am. Chem. Soc. 121 (1999) 1591–1596.
[7] M.S. Syamala, R.J. Cross, M. Saunders, J. Am. Chem. Soc. 124 (2002) 6216–6219.
[8] Y. Murata, M. Murata, K. Komatsu, Chemistry 9 (2003) 1600–1609.
[9] Y. Murata, M. Murata, K. Komatsu, J. Am. Chem. Soc. 125 (2003) 7152–7153.
[10] K. Komatsu, M. Murata, Y. Murata, Science 307 (2005) 238–240.
[11] S. Stevenson, G. Rice, T. Glass, K. Harich, F. Cromer, M.R. Jordan, J. Craft, E. Hadju, R. Bible, M.M. Olmstead, K. Maitra, A.J. Fisher, A.L. Balch, H.C. Dorn, Nature 401 (1999) 55–57.
[12] M. Krause, M. Hulman, H. Kuzmany, T.J.S. Dennis, M. Inakuma, H. Shinohara, J. Chem. Phys. 111 (1999) 7976–7984.
[13] M. Krause, H. Kuzmany, P. Georgi, L. Dunsch, K. Vietze, G. Seifert, J. Chem. Phys. 115 (2001) 6596–6605.
[14] M. Krause, M. Hulman, H. Kuzmany, O. Dubay, G. Kresse, K. Vietze, G. Seifert, C. Wang, H. Shinohara, Phys. Rev. Lett. 93 (2004) 137403.
[15] K.H. Michel, B. Verberck, M. Hulman, H. Kuzmany, M. Krause, J. Chem. Phys. 126 (2007) 064304.
[16] R.J. Cross, J. Phys. Chem. A 105 (2001) 6943–6944.
[17] H. Kruse, S. Grimme, J. Phys. Chem. C 113 (2009) 17006–17010.
[18] F. Sebastianelli, M. Xu, Y.S. Elmatad, J.W. Moskowitz, Z. Bačić, J. Phys. Chem. C 111 (2007) 2497–2504.
[19] M. Xu, F. Sebastianelli, Z. Bačić, R. Lawler, N.J. Turro, J. Chem. Phys. 128 (2008) 011101.
[20] S. Mamone, M. Ge, D. Hüvonen, U. Nagel, A. Danquigny, F. Cuda, M.C. Grossel, Y. Murata, K. Komatsu, M.H. Levitt, T. Rõõm, M. Carravetta, J. Chem. Phys. 130 (2009) 081103.
[21] M. Xu, F. Sebastianelli, B.R. Gibbons, Z. Bačić, R. Lawler, N.J. Turro, J. Chem. Phys. 130 (2009) 224306.
[22] F. Sebastianelli, M. Xu, Z. Bačić, R. Lawler, N.J. Turro, J. Am. Chem. Soc. 132 (2010) 9826–9832.
[23] R.F. Curl, J.V.V. Kasper, K.S. Pitzer, J. Chem. Phys. 46 (1967) 3220–3228.
[24] H.H. Limbach, G. Buntkowsky, J. Mathes, S. Grundemann, T. Pery, B. Walaszek, B. Chaudret, ChemPhysChem 7 (2006) 551–554.
[25] S. Flügge, Practical Quantum Mechanics, 2nd ed., Springer-Verlag, New York, 1994.
[26] V. Schettino, M. Pagliai, L. Ciabini, G. Cardini, J. Phys. Chem. A 105 (2001) 11192–11196.
[27] N.J. Turro, A.A. Marti, J.Y.C. Chen, S. Jockusch, R.G. Lawler, M. Ruzzi, E. Sartori, S.-C. Chuang, K. Komatsu, Y. Murata, J. Am. Chem. Soc. 130 (2008) 10506–10507.
[28] N.J. Turro, J.Y.C. Chen, E. Sartori, M. Ruzzi, A.A. Marti, R.G. Lawler, S. Jockusch, J. López-Gejo, K. Komatsu, Y. Murata, Acc. Chem. Res. 43 (2010) 335–345.
[29] H.P. Gush, W.F.J. Hare, E.J. Allin, H.L. Welsh, Can. J. Phys. 38 (1960) 176–193.
[30] S. FitzGerald, S. Forth, M. Rinkoski, Phys. Rev. B 65 (2002) 140302.
[31] S. FitzGerald, H. Churchill, P. Korngut, C. Simmons, Y. Strangas, Phys. Rev. B 73 (2006) 155409.
[32] R. Herman, J. Lewis, Phys. Rev. B 73 (2006) 155408.
[33] A. Borysow, L. Frommhold, W. Meyer, J. Chem. Phys. 88 (1988) 4855–4860.
[34] W. Meyer, L. Frommhold, Phys. Rev. A 34 (1986) 2771–2779.
[35] W. Meyer, L. Frommhold, Phys. Rev. A 34 (1986) 2936–2941.
[36] J.D. Poll, J.L. Hunt, Can. J. Phys. 54 (1976) 461–470.
[37] C. Hartwig, J. Vitko, Phys. Rev. B 18 (1978) 3006–3014.
[38] K.P. Huber, G. Herzberg, Molecular Spectra and Molecular Structure. IV. Constants of Diatomic Molecules, Van Nostrand Reinhold Company, New York, 1979.
[39] S.W. Lovesey, Theory of Neutron Scattering from Condensed Matter, Oxford Univerisity Press, New York, 1984.
[40] A.J. Horsewill, S. Rols, M.R. Johnson, Y. Murata, M. Murata, K. Komatsu, M. Carravetta, S. Mamone, M.H. Levitt, J.Y.C. Chen, J.A. Johnson, X. Lei, N.J. Turro, Phys. Rev. B 82 (2010) 081410.
[41] A.J. Horsewill, K.S. Panesar, S. Rols, M.R. Johnson, Y. Murata, K. Komatsu, S. Mamone, A. Danquigny, F. Cuda, S. Maltsev, M. Grossel, M. Carravetta, M. Levitt, Phys. Rev. Lett. 102 (2009) 013001.
[42] Y. Kohama, T. Rachi, J. Jing, Z. Li, J. Tang, R. Kumashiro, S. Izumisawa, H. Kawaji, T. Atake, H. Sawa, Y. Murata, K. Komatsu, K. Tanigaki, Phys. Rev. Lett. 103 (2009) 073001.
[43] Y.J. Li, X. Lei, S. Jockusch, J.Y.C. Chen, M. Frunzi, J.A. Johnson, R.G. Lawler, Y. Murata, M. Murata, K. Komatsu, N.J. Turro, J. Am. Chem. Soc. 132 (2010) 4042–4043.
[44] E. Sartori, M. Ruzzi, N.J. Turro, J.D. Decatur, D.C. Doetschman, R.G. Lawler, A.L. Buchachenko, Y. Murata, K. Komatsu, J. Am. Chem. Soc. 128 (2006) 14752–14753.
[45] J.Y.C. Chen, A.A. Martı, N.J. Turro, K. Komatsu, Y. Murata, R.G. Lawler, J. Phys. Chem. B 145 (2010) 14689–14695.
[46] E. Sartori, M. Ruzzi, N.J. Turro, K. Komatsu, Y. Murata, R.G. Lawler, A.L. Buchachenko, J. Am. Chem. Soc. 130 (2008) 2221–2225.
[47] M. Frunzi, X. Lei, Y. Murata, K. Komatsu, S.-I. Iwamatsu, S. Murata, R.G. Lawler, N.J. Turro, J. Phys. Chem. Lett. 1 (2010) 1420–1422.
[48] M. Carravetta, O.G. Johannessen, M.H. Levitt, I. Heinmaa, R. Stern, a. Samoson, a.J. Horsewill, Y. Murata, K. Komatsu, J. Chem. Phys. 124 (2006) 104507.
[49] M. Carravetta, a. Danquigny, S. Mamone, F. Cuda, O.G. Johannessen, I. Heinmaa, K. Panesar, R. Stern, M.C. Grossel, a.J. Horsewill, a. Samoson, M. Murata, Y. Murata, K. Komatsu, M.H. Levitt, Phys. Chem. Chem. Phys. 9 (2007) 4879–4894.
[50] M. Tomaselli, B.H. Meier, J. Chem. Phys. 115 (2001) 11017–11020.
[51] M. Tomaselli, Mol. Phys. 101 (2003) 3029–3051.
[52] R. Tycko, G. Dabbagh, R.M. Fleming, R.C. Haddon, A.V. Makhija, S.M. Zahurak, Phys. Rev. Lett. 67 (1991) 1886–1889.
[53] J. Kellogg, I. Rabi, N. Ramsey, J. Zacharias, Phys. Rev. 56 (1939) 728–743.
[54] N. Ramsey, Phys. Rev. 58 (1940) 226–236.
[55] F. Reif, E.M. Purcell, Phys. Rev. 91 (1953) 631–641.
[56] I. Solomon, Phys. Rev. 110 (1958) 61–65.
[57] M.S. Dresselhaus, G. Dresselhaus, P.C. Eklund, Science of Fullerenes and Carbon Nanotubes, Academic Press, New York, 1996.
[58] N.S. Sullivan, M. Devoret, B.P. Cowan, C. Urbina, Phys. Rev. B 17 (1978) 5016–5024.
[59] Lehn J.M., Supramolecular Chemistry, New York, 1995.